Nature Environment and Pollution Technology
An International Quarterly Scientific Journal

p-ISSN: 0972-6268 e-ISSN: 2395-3454	Vol. 16	No. 1	pp. 89-97	2017

Original Research Paper | Open Access

Carbon Encapsulated Zero-Valent Iron Nanoparticle Using *Abelmoschus esculentus* (Lady's Finger) Extract as an Adsorbent for Cr(VI) in Aqueous Solution

Jephin Varughese Jose, Anu Mary Ealias and M. P. Saravanakumar†
Department of Environmental and Water Resources Engineering, School of Civil and Chemical Engineering, VIT University, Vellore, India
†Corresponding author: M. P. Saravanakumar

Nat. Env. & Poll. Tech.
Website: www.neptjournal.com

Received: 15-03-2016
Accepted: 17-04-2016

Key Words:
Iron
Nanoparticle
Adsorbent
TEM
Endothermic

ABSTRACT

In this study, lady's finger carbon encapsulated zero-valent iron nanoparticle (LCINp) was synthesized and used as an adsorbent for Cr(VI) ions in aqueous solution. The material characterization was analysed using Transmission Electron Microscopy (TEM), Scanning Electron Microscopy (SEM), Fourier Transform Infrared Spectroscopy (FTIR), and X-Ray Diffraction (XRD). Factors influencing the adsorption process such as pH, adsorbent dosage, and initial Cr(VI) concentration were studied using batch sorption experiments. Langmuir, Freundlich, and Temkin isotherm models have been applied to investigate the adsorption capacity of LCINp. Pseudo-first-order, Pseudo-second order, and Elovich model have been analysed for the kinetic study. The mechanism of adsorption was examined using Boyd's model and Weber-Morris intraparticle diffusion model. The results showed that Langmuir model and Pseudo-second-order kinetic model fit well in the adsorption process. Thermodynamic analysis portrayed that the adsorption process was spontaneous and endothermic in nature.

INTRODUCTION

In recent years, the level of pollutants in water, air and soil has increased due to the developments in industrialization and urbanization (Deveci & Kar 2013). Water pollution, which results from the industrial wastewater contains a large number of toxic and hazardous materials that can be harmful to aquatic life (Ahmad 2009, Qusti 2014). Heavy metals in aqueous streams, is a major problem to the environment due to its toxicity and non-biodegradable nature which leads to various diseases and disorders by accumulating in living organisms, groundwater and soil (Deveci & Kar 2013, Mathew et al. 2013, Nemr 2009).

Among the various heavy metals, chromium is considered as one of the most harmful pollutants to nature (Deveci & Kar 2013). In aqueous environment chromium exists in two oxidation states, trivalent (Cr(III)) and hexavalent (Cr(VI)) forms. Cr(VI) is considered as more dangerous due to its carcinogenic, toxic and mutagenic properties (Albadarin et al. 2013, Oladoja et al. 2013). It can cause various diseases such as skin irritation, lung cancer, dermatitis, asthma, kidney, liver and gastric damages to human beings (Asgari et al. 2012). Leather tanning, textile dyeing, metal processing, cement manufacturing, paints and pigments and electroplating are the various industrial process that results in a generation and distribution of Cr(VI) in the surface and groundwater (Deveci & Kar 2013).

The different physical, chemical and biological treatment methods used to remove Cr(VI) ions from the environment are chemical precipitation, adsorption, ion exchange, flotation, electrocoagulation, ecological remediation, solvent extraction, sedimentation, redox, membrane separation, and ultrafiltration (Gan et al. 2015, Luo et al. 2013, Mohan & Pittman Jr. 2006). All these methods are useful in removing the pollutants, but they have some limitations such as high operational cost, production of sludge and sophisticated operation (Sun et al. 2014). Adsorption method has been extensively used in the treatment of Cr(VI) in aqueous solution because of simple design, selectivity, high efficiency, low-cost, and smooth handling (Nematollahzadeh et al. 2015, Oladoja et al. 2013). The common adsorbents used for the treatment are activated carbon, zeolite, iron oxide, graphene, and chitosan (Gan et al. 2015).

Recently, nanotechnology based techniques are used for the removal of pollutants from the environment (Trujillo-Reyes et al. 2014). This technology produces different nanoscale materials with physicochemical, optical and magnetic properties (Trujillo-Reyes et al. 2014). Nanoscale zero-valent iron nanoparticles (NZVIs) have been examined to explore their potential in remediating extensive range of

organic and inorganic pollutants in soil and groundwater (Sun et al. 2014). The studies revealed that NZVIs are efficient and economical due to the large surface area, more number of active sites and high reaction rate (Albadarin et al. 2013, Geng et al. 2009, Montesinos et al. 2014, Sun et al. 2014).

Lady's finger carbon encapsulated iron nanoparticle (LCINp) is used as the adsorbent in this study to remove Cr(VI) in aqueous solution. Lady's finger is a crop grown in different regions of the world. It is used for various purposes such as food, manufacture of medicines and production of biodiesel (Lee et al. 2014).

The main aim of this study was to explore the potential of LCINp, as a low-cost adsorbent in remediating Cr(VI) ions from aqueous solution. The adsorption mechanism was analysed using the isotherm models, kinetic models, and thermodynamic study.

MATERIALS AND METHODS

Sample preparation: The stock solution of Cr(VI) with 1000 (mg/L) concentration was prepared by dissolving the appropriate quantity of potassium dichromate ($K_2Cr_2O_7$) in double distilled water. The desired concentration of Cr(VI) standard solution was made from the stock solution. All the chemicals and reagents used are of analytical grade.

Synthesis of LCINp: The Lady's finger carbon encapsulated iron nanoparticle (LCINp) was prepared from lady's finger, which was grown in Vellore, Tamil Nadu. 150g of lady's finger was cut into small pieces and immersed in 600mL of distilled water and kept in the refrigerator for 24h. Then the extract was filtered using Whatman filter paper #1. 2g of $FeCl_3$was added to 30mL of filtered liquid and agitated continuously for 1h. After agitation, the liquid was placed in Muffle Furnace at 800°C for 1h. Preserve the LCINp produced in a desiccator for the future use.

Adsorption experiments: The batch sorption experiments were carried out in 250mL Erlenmeyer flask containing 100mL Cr(VI) solution of 100mg/L concentration with an adsorbent dosage of 0.1g LCINp. It was shaken for 2h at 140rpm using an orbital shaker. After treatment, the solution was filtered through Whatman #41 filter paper and the total and hexavalent chromium of the filtrate were estimated using Atomic Adsorption Spectroscopy (AAS; Perkin-Elmer 2380) and UV-Visible Spectrophotometer (Cyberlab-double beam) at a wavelength of 540nm (Zhang et al. 2015). The isotherm and kinetic models were evaluated using the optimized pH and adsorbent dosage ranging from 0.05 to 0.2g at various time intervals from 10 to 180min.

Material characterization: The surface morphology of the sample was studied using Scanning Electron Microscopy (SEM, Carl Zeiss, EVO 18) equipped with Energy Dispersive Spectrometer (EDS, Oxford PentaFetx5) and Transmission Electron Microscopy (TEM, JOEL USA, JEM 2100 PLUS). X-Ray Diffraction (XRD) in a Bruker advanced diffractometer was used to analyse the mineralogical properties of LCINp. The functional group analysis for the LCINp was carried out in Avator-330 FTIR spectrometer.

RESULTS AND DISCUSSION

Characteristics of adsorbent: The morphological characteristics of LCINp were analysed using TEM and SEM-EDX. The results of TEM (Fig. 1a) portray the presence of very fine and spherical shape nano particles with size ranging from 10 to 50nm. The SEM-EDX analysis before and after the treatment (Fig.1b and 1c) depict that LCINp surface has porous structure and indicates the presence of carbon, iron, oxygen and chromium.

The XRD analysis of LCINp before and after treatment is shown in Fig. 1d and 1e. The absence of distinctive peaks reveals the amorphous nature of LCINp. The diffraction peak of 2θ at 44.71 indicates the presence of zero-valent (α-Fe) iron nano particle (Madhavi et al. 2013, Singh et al. 2011). The peaks at 2θ value of 29.98, 35.54, 35.66, 62.51 indicate FeO (OH), $FeCr_2O_4$, Maghemite (γ-Fe_2O_3) and Hematite (Sun et al. 2014).

The FTIR spectra (Fig. 1f and 1g) shows the functional group analysis before and after adsorption. The absence of peaks in the wave range 2300-2100cm^{-1} suggests that LCINp may contain only small amount of alkyne and nitrile groups. The stretching and vibration of C-O and N-H elements are ascribed in the peaks 1300-1200cm^{-1} and 1200-1000cm^{-1}. Peaks observed in 1500-400cm^{-1} is assigned to all manner of bending vibrations in the molecule. (Moradi et al. 2015, Prasad et al. 2014).

Effect of variables on adsorption process: The impact of pH on the adsorption process is studied in the range 2-10. The result (Fig. 2a) shows that the removal efficiency decreased from 87.1 to 29% as the pH increased from 2-10. The surface of the adsorbent gets protonated at low pH values, and this produces a strong attraction force between the oxy anions and a positively charged adsorbent surface, which results in maximum removal efficiency of Cr(VI) at pH 2 (Saravanakumar & Phanikumar 2013).

The influence of adsorbent dosage on the treatment process is studied in the range of 0.05g to 0.15g per 100mL solution. The result (Fig. 2b) portrays that as the adsorbent dosage increases, the removal efficiency increased from 58.1 to 87.1%. The increase in LCINp dosage increases the availability of active sites thus results in high removal efficiency

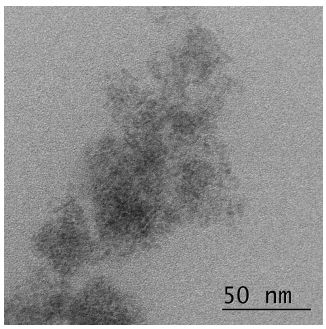

Fig. 1a: TEM image of LCINp.

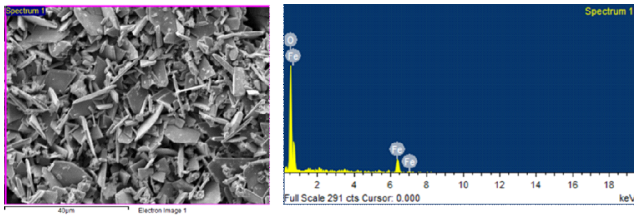

Fig. 1b: SEM and EDX spectra of LCINp before treatment.

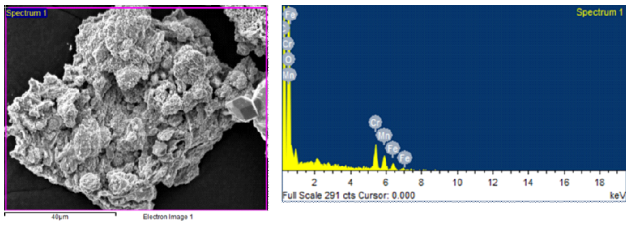

Fig. 1c: SEM and EDX spectra of LCINp after treatment.

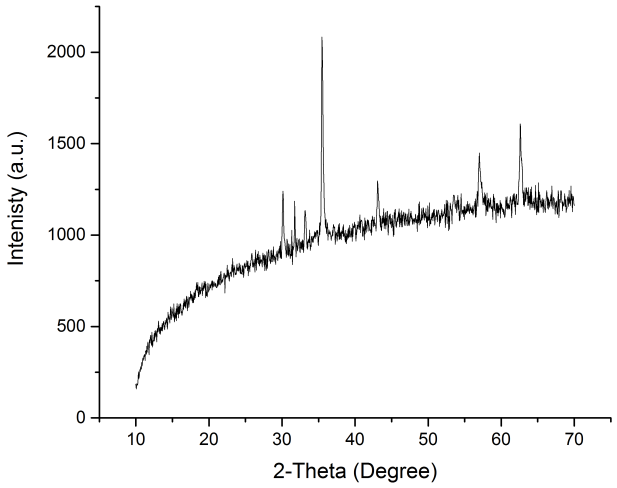

Fig. 1d: XRD spectra of LCINp before treatment.

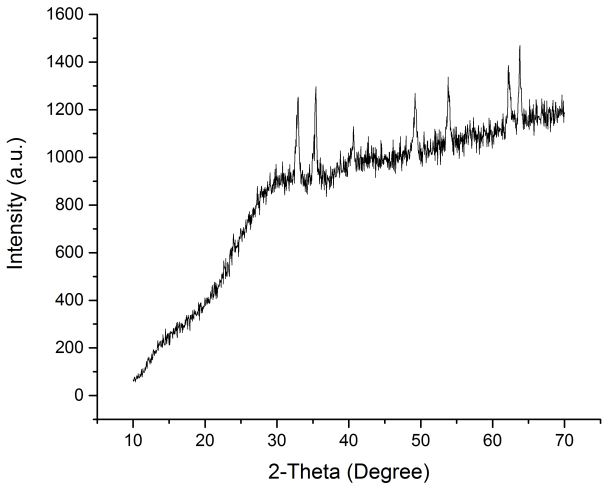

Fig. 1e: XRD spectra of LCINp after treatment.

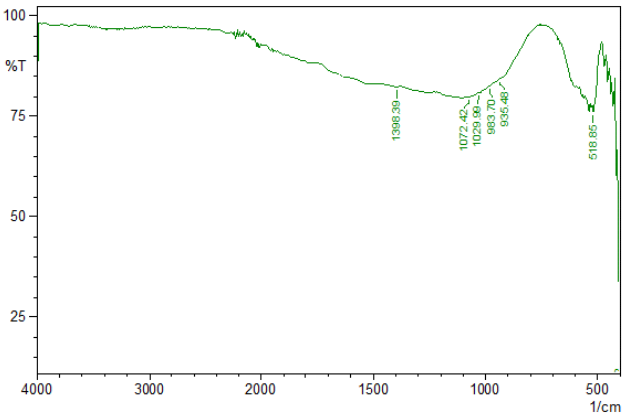

Fig. 1f: FTIR spectra of LCINp before treatment.

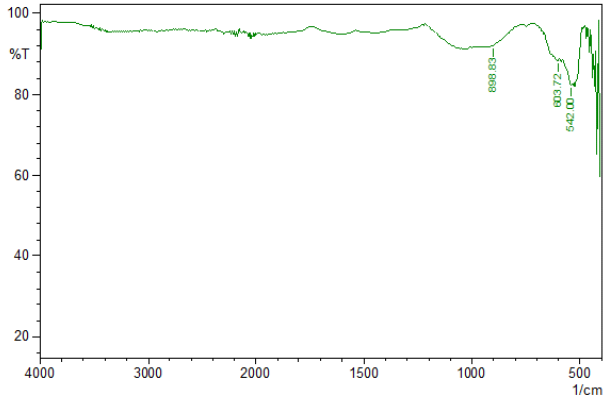

Fig. 1g: FTIR spectra of LCINp after treatment.

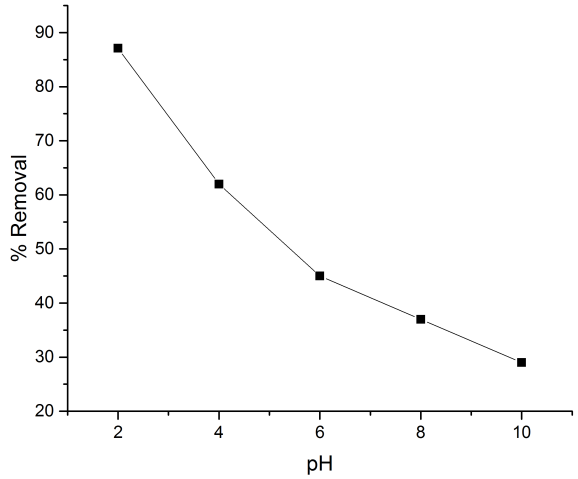

Fig. 2a: Effect of pH on LCINp.

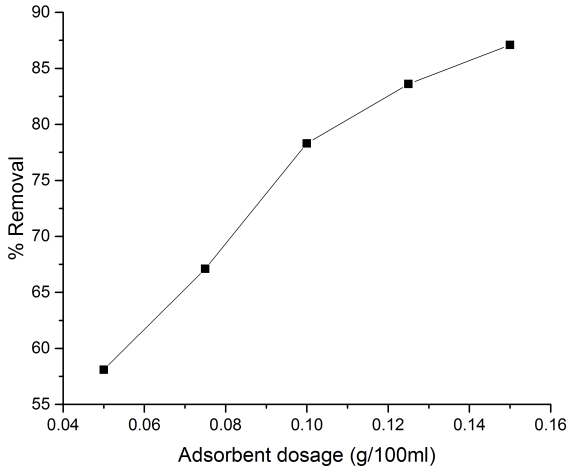

Fig. 2b: Effect of adsorbent dosage.

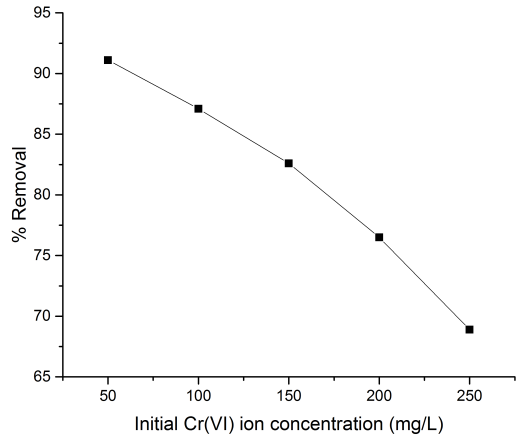

Fig. 2c: Effect of initial Cr(VI) concentration.

of Cr(VI) ions from aqueous solution (Deveci & Kar 2013).

The effect of initial Cr (VI) concentration on the adsorption process was studied in the range of 50-250mg/L at the optimized dosage and pH conditions. The results (Fig. 2c) depict that the removal efficiency decreased from 91.1 to 68.9 as the initial concentration increases due to the saturation of available active sites by the Cr(VI) ions (Vilvanathan & Shanthakumar 2015).

Adsorption isotherm study: The data obtained from batch sorption experiments are modelled with different isotherm models such as Langmuir, Freundlich, and Temkin. Isotherm study describes the interaction of adsorbate with the adsorbent and mechanism of adsorption (Tan et al. 2015). The isotherm constants are calculated from Langmuir, Freundlich, and Temkin isotherm models and shown in Table 1.

Langmuir isotherm model assumes that removal of the sorbate occurs on the homogeneous surface by monolayer adsorption with constant binding energy and ions have an equal affinity towards the adsorbent site on the surface of adsorbent (Vilvanathan & Shanthakumar 2015). The type (II), linear expression of Langmuir isotherm model (Eq. 1), was used in this study, and the graph (Fig. 3a) plotted $1/q_e$ vs. $1/C_e$(Kayranli 2011).

$$\frac{1}{q_e} = \frac{1}{q_{max} K_L C_e} + \frac{1}{q_{max}} \quad ...(1)$$

Where, q_e is the amount of Cr(VI) adsorbed at equilibrium (mg/g), q_{max} is maximum adsorption capacity of LCINp (mg/g), C_e is the equilibrium concentration of Cr(VI) (mg/L), and K_L is Langmuir isotherm constant (L/mg). The dimensionless separator factor R_L has been used for checking the feasibility of Langmuir isotherm and calculated from the following equation (Eq. 2).

$$R_L = \frac{1}{1 + K_L C_0} \quad ...(2)$$

Where, K_L is Langmuir isotherm constant (L/mg) and C_0 is initial concentration (mg/L). From Table 1, the value of R_L for LCINp lies in between 0 and 1 which indicates that the adsorption isotherm is favourable. The maximum adsorption capacity of LCINp is 172.414mg/g (Table 1) which exhibits a good adsorption performance.

The Freundlich isotherm is an empirical model and describes the heterogeneous adsorption model with different energies of sorption. The adsorbent surface has different functional groups having a different preference for the adsorbate (Vilvanathan & Shanthakumar 2015). The following equation describes this model (Eq. 3) and the graph

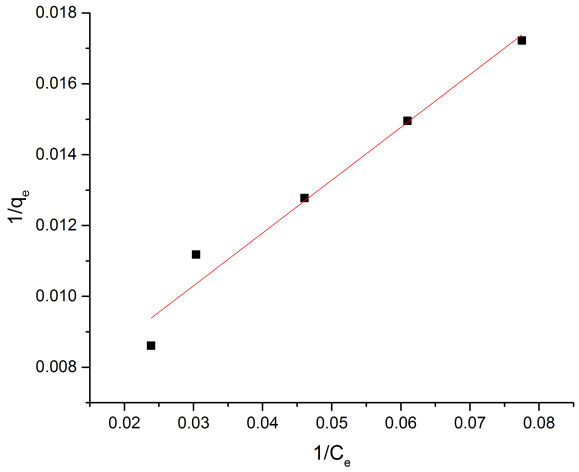

Fig. 3a: Langmuir isotherm.

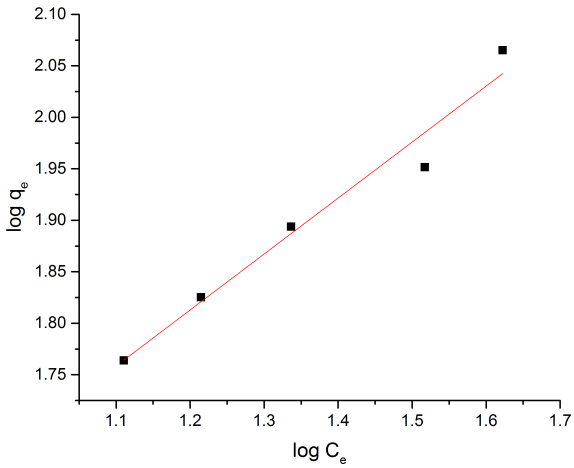

Fig. 3b: Freundlich isotherm.

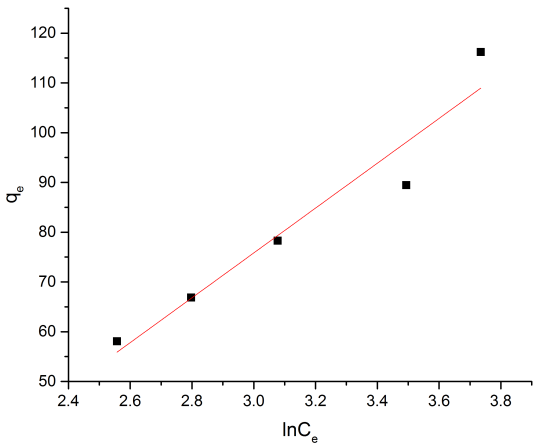

Fig. 3c: Temkin isotherm.

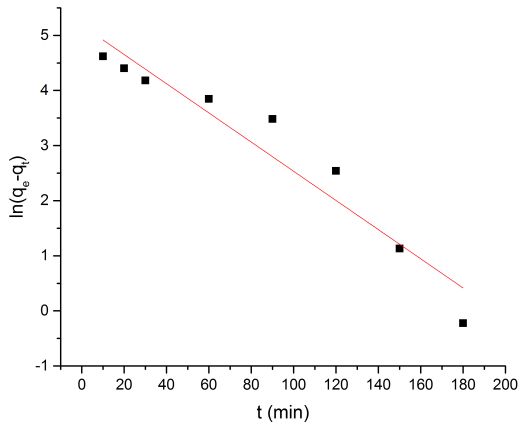

Fig. 3d: Pseudo-first order kinetics.

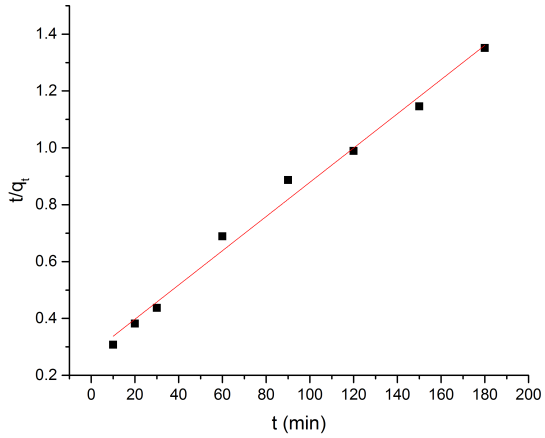

Fig. 3e: Pseudo-second order kinetics.

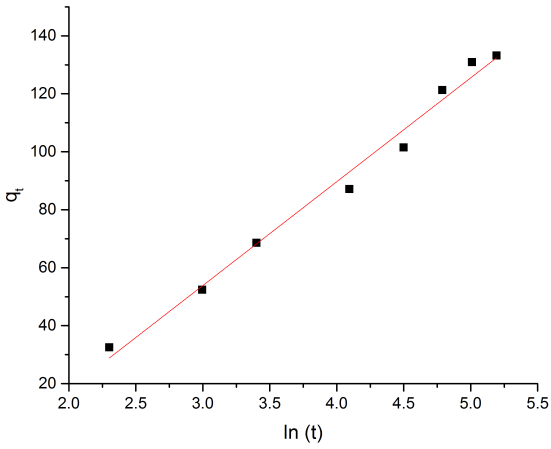

Fig. 3f: Elovich model.

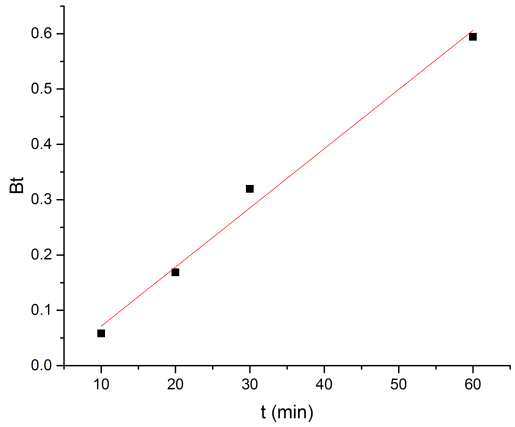

Fig. 3g: Boyd plot.

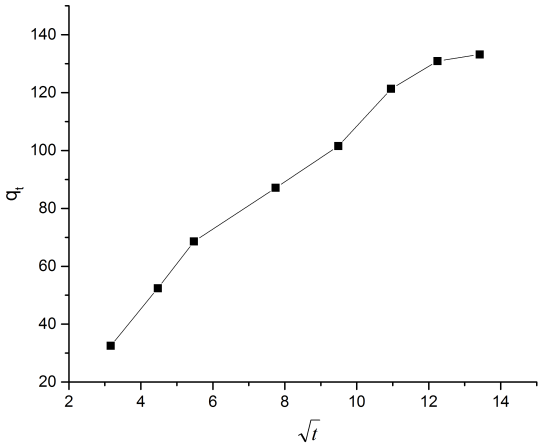

Fig. 3h: Weber-Morris intraparticle diffusion model.

(Fig. 3.b) plotted log q_e vs. log C_e(Kayranli 2011).

$$\text{Log}\, q_e = logK_F + \frac{1}{n} logC_e \quad ...(3)$$

Where, C_e is the equilibrium concentration of Cr(VI) (mg/L), q_e is the amount of Cr(VI) adsorbed at equilibrium (mg/g), n is the Freundlich linearity constant, and K_F is Freundlich constant (L/g). From the Table 1, n value in Freundlich model isotherm of LCINp is greater than 1 and ranges between 1 and 10 which concludes that chemical adsorption process occurs naturally for the removal of Cr(VI) and represent favourable adsorption condition.

Temkin equation based on the effect of some direct adsorbate-adsorbent relation on the sorption isotherm, and due to interactions, the decrease in the heat of adsorption of the adsorbate, is linear. The following equation (Eq. 4) describes this model and the graph (Fig. 3c) plotted q_e vs. ln C_e(Kayranli 2011).

Table 1: Isotherm parameters of LCINp.

Isotherms Models	Isotherm Constants	LCINp
Langmuir	q_{max}, mg/g	172.414
	K_L, L/mg	0.0389
	R_L	0.2043
	R^2	0.9704
Freundlich	K_F, L/g	14.4743
	n	1.8399
	R^2	0.9683
Temkin	B, J/mol	55.3602
	K_T, L/g	0.2679
	R^2	0.9352

Table 2: Kinetic parameters of LCINp.

Kinetic Models	Kinetic Constants	LCINp
Pseudo-first order	k_1 (min^{-1})	0.0265
	q_e (mg/g)	178.074
	R^2	0.9321
Pseudo-second order	k_2 (min^{-1})	1.299×10^{-4}
	q_e (mg/g)	166.66
	R^2	0.9902
Elovich	β (g/mg)	0.0279
	α (mg/g/min)	8.015
	R^2	0.9873

$$q_e = \frac{RT}{A_T} ln K_T + \frac{RT}{A_T} ln C_e \quad ...(4)$$

Where, C_e is the equilibrium concentration of Cr(VI) (mg/L), R is ideal gas constant (J/K/mol), T is temperature (K), K_T is Tempkin isotherm constant (L/g).

The results of the isotherm model conclude that Langmuir isotherm fits best for the removal of Cr(VI) ions using LCINp hence, monolayer adsorption and chemisorption favors the adsorption process.

Kinetic study: The adsorption kinetics of Cr(VI) ions were analysed using Lagergren's pseudo-first order kinetic model, pseudo-second-order kinetic model, and Elovich's kinetic model. The kinetic study gives information in selecting the optimum operation conditions, and it predicts the adsorption rate that uses in designing and modelling the process (Nemr 2009).

Lagergren's pseudo-first order kinetic model explains the adsorption rate based on the adsorption capacity (Vilvanathan & Shanthakumar 2015). The linear equation (Eq. 5) expressed as,

$$\ln(q_e - q_t) = lnq_e - k_1 t \quad ...(5)$$

Where, q_e is the amount of Cr(VI) adsorbed at equilibrium (mg/g), q_t is the amount of Cr(VI) adsorbed at the time, t

Table 3: Thermodynamic parameters of LCINp.

Biosorbent	Temperature (K)	Thermodynamic Parameters			
		Δ H° (KJ/mol)	Δ S° (KJ/mol/K)	Δ G°(KJ/mol)	R^2
LCINp	300	24.138	0.103	-6.831	0.9787
	313			-8.173	
	323			-9.205	

(mg/g), k_1 is pseudo-first order kinetic model constant (min^{-1}). The k_1 and q_e values are determined from the slope and intercept of the plotted log (q_e - q_t) vs. t and represented in Fig. 3d.

Pseudo-second order kinetic model assumes that chemisorption of the adsorbate takes place on the adsorbent (Kayranli 2011). The linear equation of type I (Eq. 6) can express as,

$$\frac{1}{q_t} = \frac{1}{k_2 q_e^2} + \frac{t}{q_e} \quad ...(6)$$

Where, q_e is the amount of Cr(VI) adsorbed at equilibrium (mg/g), q_t is Cr(VI) ions amount adsorbed at the time, t (mg/g), k_2 is pseudo-second order kinetic model constant (min^{-1}). The values of $k_2$and q_e are determined from the slope and intercept of the plot t/$q_t$vs. t and represented in Fig. 3e.

The Elovich's kinetic model assumes that adsorbent surface is having heterogeneous active sites with different activation energy during the adsorption of organic compounds (Kayranli 2011). The linear equation (Eq. 7) for the model expressed as,

$$q_t = \frac{1}{\beta}\ln(\propto \beta) + \frac{1}{\beta}\ln t \quad ...(7)$$

Where, t (mg/g), $\propto$ is initial adsorption rate constant (mg/g/min) and β is related to the extent of surface coverage and activation energy for chemisorption (g/mg) and q_t is the amount of Cr(VI) adsorbed at time. The slope and intercept of the plot q_t vs. ln t in Fig. 3f gives the values of model constants $\propto$ and β (Errais et al. 2011).

Three different kinetic models applied in this study, and the calculated statistic parameters reported in Table 2. Based on the correlation coefficient value R^2, the kinetics of adsorption of Cr(VI) ions by LCINp are well described by pseudo-second-order > elovich > pseudo-first-order equation. The result confirms that the overall rate of adsorption process controlled by chemisorption that involves sharing or exchange of electrons using valence forces between the adsorbent and adsorbate (Elkady et al. 2011).

Mechanism of adsorption process: The mechanism of adsorption is studied using the Boyd's model and Weber-Morris intraparticle diffusion model. Boyd's model used in predicting the mechanism of adsorption process by plotting Bt vs. t (time), where Bt is a function of F (Eq. 8) (Hameed & El-Khaiary 2008).

$$F = \frac{q_t}{q_e} \quad ...(8)$$

Where, F is the fractional attainment of equilibrium at different times, t, q_t and q_e (mg/g) are the Cr(VI) ions uptake at time t and equilibrium. The following approximations (Eqs. 9 and 10) are used to calculate the Bt values corresponding to F values by applying the Fourier transform and then integration (Hameed & El-Khaiary 2008),

$$\text{for F values} > 0.85,\ Bt = -0.4977 - \ln(1 - F) \quad ...(9)$$

$$\text{and for F value} < 0.85,\ Bt = \left(\sqrt{\pi} - \sqrt{\pi - \left(\frac{\pi^2 F}{3}\right)}\right)^2 \quad ...(10)$$

If the plot Bt vs. t is linear and passes through the origin, then pore diffusion controls the mass transfer rate, and if the plot is linear or nonlinear and does not pass through the origin, then film-diffusion or chemical reaction controls the rate of adsorption (Hameed & El-Khaiary 2008). Fig. 3g shows the Boyd plot for the first 60min of adsorption, and it shows nonlinear segment without passing through the origin that suggests that film diffusion or chemical reaction controls the rate of adsorption of Cr(VI) ions by LCINp during this period.

Weber-Morris intraparticle diffusion model is derived from Fick's second law of diffusion (Hameed & El-Khaiary 2008). The following is the linear equation (Eq. 11) of the model,

$$q_t = k_{id} t^{0.5} + c \quad ...(11)$$

Where, q_t denotes the amount of Cr(VI) adsorbed at the time, t (mg/g), k_{id} denotes intraparticle diffusion rate constant (mg/g/min^{-1}). If the plot q_t vs. t is linear and passes through the origin with the slope equals to k_{id} and intercept equal to zero, then pore diffusion is the rate-limiting step (Hameed & El-Khaiary 2008).

The plot (Fig. 3h) shows that it is multilinear with three linear segments with the intercept values significantly dif-

ferent from zero which suggests that pore diffusion does not control the overall rate of adsorption of Cr(VI) ions using LCINp. It concludes that the first linear segment represents film-diffusion or chemical reaction, the second linear segment represents pore diffusion, and the final segment represents equilibrium diffusion.

Thermodynamic study: Thermodynamic studies have been done at the optimum dosage and pH condition for varying temperatures 300K, 313K, and 323K. The thermodynamic parameters that considered for the adsorption study are standard free energy (ΔG^o), standard enthalpy (ΔH^o) and standard entropy (ΔS^o) (Elkady et al. 2011). The values of standard entropy and standard enthalpy have been calculated using the following equation (Eq. 12):

$$lnk_d = \frac{\Delta S^o}{R} - \frac{\Delta H^o}{RT} \quad ...(12)$$

Where, R is the universal gas constant (8.314 J/molK), k_d is the distribution coefficient, and T is the absolute solution temperature in Kelvin. The slope and intercept of the graph lnk_d vs. 1/T give the values of ΔH^o and ΔS^o.

The standard free energy is calculated using the equation (Eq. 13),

$$\Delta G^o = -RT \ln k_d \quad ...(13)$$

The calculated values of ΔH^o, ΔS^o, and ΔG^o listed in Table 3. The positive value of ΔH^o indicates that adsorption process is endothermic in nature and the adsorption of Cr(VI) ions onto the adsorbents increases at a higher temperature. The positive value of ΔS^o shows the affinity of LCINp for Cr(VI) ions and the increased randomness at the solid-solution interface during the adsorption process. The negative values of ΔG^o indicate that the adsorption of Cr(VI) ions onto the LCINp are more favourable at a higher temperature, and it also shows the feasibility and spontaneous nature of the adsorption process.

CONCLUSION

In this study, the carbon encapsulated zero-valent iron nanoparticle, biosynthesized using lady's finger, has been reported. TEM and SEM images have revealed that the average size of nanoparticles is less than 100nm. The XRD results have shown that zerovalent iron nanoparticles are present in the LCINp. The Langmuir isotherm and pseudo-second-order kinetic model fit well for the adsorption process with shows chemisorption of the adsorbate take place on the adsorbent. The mechanism of adsorption revealed that film diffusion occurs, and thermodynamic study demonstrated that the adsorption process is endothermic and spontaneous in nature. The experimental and instrumental analysis have shown that LCINp can be used as a nano-adsorbent for the removal of Cr(VI) ions in aqueous solution.

ACKNOWLEDGEMENT

The authors would like to thank the VIT University, Vellore for providing the necessary facilities and infrastructure to carry out this work

REFERENCES

Ahmad, R. 2009. Studies on adsorption of crystal violet dye from aqueous solution onto coniferous pinus bark powder (CPBP). Journal of Hazardous Materials, 171: 767-73.

Albadarin, A.B., Yang, Z., Mangwandi, C., Glocheux, Y., Walker, G., and Ahmad, M.N.M. 2013. Experimental design and batch experiments for optimization of Cr(VI) removal from aqueous solutions by hydrous cerium oxide nanoparticles. Chemical Engineering Research and Design, 92(7): 1354-1362.

Asgari, G., Rahmani, A.R., Faradmal, J. and Mohammadi, A.M.S. 2012. Kinetic and isotherm of hexavalent chromium adsorption onto nano hydroxyapatite. Journal of Research in Health Sciences, 12: 45-53.

Deveci, H. and Kar, Y. 2013. Adsorption of hexavalent chromium from aqueous solutions by bio-chars obtained during biomass pyrolysis. Journal of Industrial and Engineering Chemistry, 19: 190-96.

Elkady, M.F., Ibrahim, A.M. and Abd El-Latif El-Latif, M.M. 2011. Assessment of the adsorption kinetics, equilibrium and thermodynamic for the potential removal of reactive red dye using eggshell biocomposite beads. Desalination, 278: 412-23.

Errais, E., Duplay, J., Darragi, F., Rabet, I.M., Aubert, A., Huber, F., and Morvan, G. 2011. Efficient anionic dye adsorption on natural untreated clay: Kinetic study and thermodynamic parameters. Desalination, 275: 74-81.

Gan, C., Liu, Y., Tan, X., Wang, S., Zeng, G., Zheng, B., Li, T., Jiang, Z. and Liu, W. 2015. Effect of porous zinc-biochar nanocomposites on Cr(VI) adsorption from aqueous solution. RSC Advances, 10.1039/C5RA04416B

Geng, B., Jin, Z., Li, T. and Xinhua, Qi. 2009. Preparation of chitosan-stabilized FeO nanoparticles for removal of hexavalent chromium in water. Science of the Total Environment, 407: 4994-5000.

Hameed, B.H. and El-Khaiary, M.I. 2008. Malachite green adsorption by Rattan sawdust/: Isotherm, kinetic and mechanism modeling. Journal of Hazardous Materials, 159: 574-79.

Kayranli, B. 2011. Adsorption of textile dyes onto iron based waterworks sludge from aqueous solution; isotherm, kinetic and thermodynamic study. Chemical Engineering Journal, 173: 782-91.

Lee, L.Y., Chin, D.Z.B., Lee, X.J., Chemmangattuvalappil, N. and Gan, S. 2014. Evaluation of abelmoschus esculentus (lady's finger) seed as a novel biosorbent for the removal of acid blue 113 dye from aqueous solutions. Process Safety and Environmental Protection, 94: 329-338.

Luo, C., Tian, Z., Yang, B., Zhang, L. and Yan. S. 2013. Manganese dioxide / iron oxide / acid oxidized multi-walled carbon nanotube magnetic nanocomposite for enhanced hexavalent chromium removal. Chemical Engineering Journal, 234: 256-65.

Madhavi, V., Prasad, T.N.V.K.V, Reddy, A.V.B., Reddy, B.R. and Madhavi, G. 2013. Molecular and biomolecular spectroscopy application of phytogenic zerovalent iron nanoparticles in the adsorption of hexavalent chromium. Spectrochimica Acta - Part

A: Molecular and Biomolecular Spectroscopy, 116: 17-25.

Mathew, R.M., Arthy, M., Saravanakumar, M.P. and Balamurali Krishna, C. 2013. Removal of hexavalent chromium from aqueous solution by adsorption on raw powder and chemically activated carbon of hibiscus rosa-sinensis flowers. Nature Environmnt and Pollution Technology, 12: 475-78.

Mohan, D. and Pittman, Jr., C.U. 2006. Activated carbons and low cost adsorbents for remediation of tri- and hexavalent chromium from water. Journal of Hazardous Materials, 137: 762-811.

Montesinos, V.N., Quici, N., Halac, E.B., Layva, A.G., Custo, G., Beingo, S., Zampieri, G. and Litter, M.I. 2014. Highly efficient removal of Cr (VI) from water with nanoparticulated zerovalent iron/ : Understanding the Fe(III)-Cr(III) passive outer layer structure. Chemical Engineering Journal, 244: 569-75.

Moradi, O., Gupta, V.K., Agarwal, S., Tyagi, I., Asif, M., Makhlouf, A.S.H., Sadegh, H. and Shahryari-Ghoshekandi, R. 2015. Characteristics and electrical conductivity of graphene and graphene oxide for adsorption of cationic dyes from liquids/ : kinetic and thermodynamic study. Journal of Industrial and Engineering Chemistry, 28: 294-301.

Nematollahzadeh, A., Seraj, S. and Mirzayi, B. 2015. Catecholamine coated maghemite nanoparticles for the environmental remediation/ : Hexavalent chromium ions removal. Chemical Engineering Journal, 277: 21-29.

Nemr, A.E. 2009. Potential of pomegranate husk carbon for Cr (VI) removal from wastewater: Kinetic and isotherm studies. Journal of Hazardous Materials, 161: 132-41.

Oladoja, N.A., Ololade, I.A., Alimi, O.A., Akinnifesi, T.A. and Olaremu, G.A. 2013. Iron incorporated rice husk silica as a sorbent for hexavalent chromium attenuation in aqueous system. Chemical Engineering Research and Deisgn, 91: 2691-2702.

Prasad, K.S., Gandhi, P. and Selvaraj, K. 2014. Synthesis of green nano iron particles (GnIP) and their application in adsorptive removal of As(III) and As(V) from aqueous solution. Applied Surface Science, 317: 1052-1059.

Qusti, A.H. 2014. Removal of chromium (VI) from aqueous solution using manganese oxide nanofibers. Journal of Industrial and Engineering Chemistry, 20(5): 3394-3399.

Saravanakumar, M.P. and Phanikumar, B.R. 2013. Response surface modelling of Cr^{6+} adsorption from aqueous solution by neem bark powder: Box-Behnken experimental approach. Environmental Science and Pollution Research, 20: 1327-43.

Singh, R., Misra,V., and Singh, R.P. 2011. Synthesis, characterization and role of zero-valent iron nanoparticle in removal of hexavalent chromium from chromium-spiked soil. J. Nanopart. Res., 13:4063-4073.

Sun, X., Yan, Y., Li, J., Han, W. and Wang, L. 2014. SBA-15-Incorporated nanoscale zero-valent iron particles for chromium (VI) removal from groundwater/ : Mechanism, effect of pH, humic acid and sustained reactivity. Journal of Hazardous Materials, 266:26-33.

Tan, X., Liu, Y., Zeng, G., Wang, X., Hu, X., Gu, Y. and Yang, Z. 2015. Application of Biochar for the removal of pollutants from aqueous solutions.Chemosphere.http://dx.doi.org/10.1016/j.chemosphere.2014.12.058

Trujillo-Reyes, J., Peralta-Videa, J.R. and Gardea-Torresdey, J.L. 2014. Supported and unsupported nanomaterials for water and soil remediation/: Are they a useful solution for worldwide pollution? Journal of Hazardous Materials, 280:487-503.

Vilvanathan, S. and Shanthakumar, S. 2015. Biosorption of Co(II) ions from aqueous solution using *Chrysanthemum indicum*/ : Kinetics, equilibrium and thermodynamics. Process Safety and Environmental Protection, 96:98-110.

Zhang, M., Liu, Y., Li, T., Xu, W., Zheng, B., Tan, X., Wang, H., Guo, Y., Guo, F. and Wang, S. 2015. Chitosan modification of magnetic Biochar produced from *Eichhornia crassipes* for enhanced sorption of Cr(VI) from aqueous solution. RSC Advances, 5: 46955-64.